Marine and Petroleum Geology 73 (2016) 392–404

Contents lists available at ScienceDirect

Marine and Petroleum Geology

journal homepage: www.elsevier.com/locate/marpetgeo

Research paper

Effect of kerogen on rock physics of immature organic-rich chalks

Omri Shitrit [a], Yossef H. Hatzor [a, *], Shimon Feinstein [a], Vyacheslav Palchik [a], Harold J. Vinegar [a, b]

[a] Department of Geological Environmental Sciences, Ben-Gurion University of the Negev, Beer-Sheva 84105, Israel
[b] Israel Energy Initiatives Ltd., 5 Shlomo HaLevi Street, Jerusalem 91450, Israel

ARTICLE INFO

Article history:
Received 5 January 2016
Received in revised form
17 March 2016
Accepted 19 March 2016
Available online 22 March 2016

Keywords:
Organic-rich chalk
Source rock
Porosity
Kerogen
Acoustic velocity
Poroelasticity
Tensile strength
Compressive strength

ABSTRACT

We study the rock physics of organic-rich chalk from the Shefela basin, central Israel, based on laboratory measurements of core material from the Zoharim well. This deposit is an immature source rock that includes the Late Cretaceous Ghareb and Mishash formations. The studied rock is composed of three dominating phases: minerals, kerogen, and pores. We investigate how porosity and kerogen influence the physical behavior of the rock, based on measurements of porosity, density, acoustic velocities, elastic moduli, tensile strength and compressive strength. We find that the dynamic bulk modulus and the static Young's modulus decrease with increasing kerogen content as well as with increasing porosity. To describe the stiffness of the solid skeleton we use two different poroelasticity models for fluid substitution assuming material isotropy: Biot-Gassmann model and Marion's BAM model. The obtained poroelasticity coefficients indicate a soft matrix composed of kerogen-micrite mixture, characterized by a low BAM normalized stiffness factor ($w \sim 0.2$) and a high Biot coefficient ($\beta \sim 0.9$). These values appear to vary with changes in kerogen content, grain size and degree of cementation. Porosity, which typically decreases with depth in the studied basin, does not show a clear correlation with kerogen content. Moreover, both compressive and tensile strengths decrease linearly with increasing porosity, regardless of kerogen content. We use a density–kerogen relationship to create a porosity depth profile, by combining data from continuous cores and density well logs. By comparing sonic logs with laboratory measurements of P-wave velocities on fully-saturated cores, we are able to detect a gas zone in the shallow interval of the sequence in the studied well.

1. Introduction

Organic-rich sediments are widely known as source rocks due to their high potential within the organic matter to produce oil and gas. These rocks are typically fine-grained sediments that include organic matter in solid and fluid states. Kerogen is solid, and is the most abundant organic phase in thermally immature source rocks. The physical properties of source rocks are strongly influenced by kerogen properties such as density, maturity level, chemical composition, elastic moduli and acoustic velocities. The advance in production technologies allows now to produce oil and gas from immature source rocks via in situ methods for inducing maturation. Moreover, tight source rocks may also contain producible hydrocarbons. These aspects, among others, motivate the study of rock physics of immature organic-rich rocks.

Several studies of rock physics of source rocks have been conducted (e.g. Bisnovat et al., 2015; Carcione, 2000; Pinna et al., 2011; Sayers, 2013; Vernik and Nur, 1992). These rocks often exhibit low permeability, low density, slow acoustic waves, mechanical softness, and porosity typically ranges from 0.5% to 45% (e.g. Bisnovat et al., 2015; Vernik and Nur, 1992). The mineralogical phase of source rocks is frequently occupied by shales, with illite being the most abundant mineral (Carcione, 2000). A model proposed by Vernik and Landis (1996) suggests that kerogen is isotropic whereas shales are transversely isotropic, thus suggesting that the entire medium is transversely isotropic. This may not be the case where the clay content is low, and the predominant minerals are quartz or carbonates (Carcione et al., 2011). Anisotropy stems from different origins, such as interlayering of lithologies, preferred orientation of minerals, and cracks induced by stresses or hydrocarbon expulsion (Vernik and Nur, 1992). Chalks are among the less studied organic-rich sediments, specifically in the field of rock

* Corresponding author.
E-mail address: hatzor@bgu.ac.il (Y.H. Hatzor).

http://dx.doi.org/10.1016/j.marpetgeo.2016.03.023
0264-8172/

physics, because rarely have they been identified as potential source rocks. Anisotropy in chalks is different than in shales due to differences in mineralogy and fabric. Consequently, the physical behavior of organic-rich chalks combines characteristics of non-organic chalks and organic-rich shales.

Organic-rich shales typically exhibit strong velocity anisotropy, low velocity in the bedding-normal direction, and relatively low density and porosity (Vernik and Milovac, 2011). These rocks are transversely isotropic with the symmetry axis in the bedding-normal direction, and can be described by five elastic constants: C_{11}, C_{33}, C_{55}, C_{66}, and C_{13} (for full definitions see Pinna et al., 2011; or Sayers, 2013). The Bakken shale is a case in point of rock physics of transversely isotropic source rocks (e.g. Carcione et al., 2011; Sayers, 2013; Vernik and Nur, 1992). Shale fabric is conceptualized as lenticular grains of illite rather than continuous sheets (Vernik and Landis, 1996; Vernik and Milovac, 2011). Sayers (2013) concluded that the kerogen in the Bakken reduces elastic stiffnesses when forms an interconnected network instead of discrete inclusions. Carcione et al. (2011) indicated that if kerogen is treated as part of the solid skeleton, it is optional to model the effective moduli using Hashin-Shtrikman bounds (Hashin and Shtrikman, 1963). Although Gassmann's theory is frequently used for predicting elastic moduli, it is noteworthy that organic-rich rocks do not obey some basic assumptions of that theory (Gassmann, 1951; Mavko et al., 2009). For example, not all skeletal components have the same bulk and shear moduli, and usually organic-rich rocks contain clays that may exhibit matrix anisotropy and non-negligible hygroscopy. Furthermore, Gassmann's theory assumes the pore pressure is equilibrated throughout the pore space, and that might not be the case where wave frequencies are higher, such as in laboratory ultrasonic devices or sonic well logs (Mavko et al., 2009). However, modifications of Gassmann's theory can lead to more accurate results, for example in cases of mixed mineralogy (Brown and Korringa, 1975) or by empirical models for specific lithologies (Krief et al., 1990).

Anisotropy of high-porosity chalks may be exhibited by parameters such as permeability, strength, elasticity and acoustic velocities. Korsnes et al. (2008) studied the Stevns Klint and Liege outcrop chalks, and reported isotropic permeability (1–4 mD) and tensile strength (0.5–0.58 MPa), but anisotropy in compressive strength and bulk modulus. Stevns Klint chalk exhibits greater stiffness parallel to bedding but the Liege chalk is stiffer normal to bedding. Talesnick, Hatzor and Tsesarsky (2001) found that compressive strength in the bedding-parallel direction is ~1.5 times greater than in the bedding-normal direction in the high-porosity transversely isotropic Marasha chalk, regardless of the water content in the range of 0-50%. Bisnovat et al. (2015) studied the mechanical and petrophysical properties of the organic-rich chalk in the Shefela basin which is also studied here, using cores from the Aderet well. They found that tensile strength ratios parallel/normal to bedding are 1.7 and 2.2 in the Ghareb and Mishash formations, respectively. Compressive strength was found to be positively correlated with total organic carbon (TOC), but porosity, permeability, tensile strength and static elastic moduli were not, despite of the high organic content (TOC up to 20%). It was also noted that the chalk exhibited brittle behavior at room conditions.

Chalks are typically highly porous, with a small pore size at the micro to nano meter scale, so that chalk physics depends strongly on pore-scale mechanisms. The Niobrara chalk in Denver basin contains a type II kerogen with TOC amounts of ~3.2% (Rice, 1986). There, the porosity decreases consistently with depth, from 45% at 300 m depth to ~5% at 2100 m (Lockridge and Pollastro, 1988). High porosity in chalks can be found even at great depths, as in the Tor and Ekofisk formations from the North Sea (Japsen et al., 2004), where porosity of 45% at 3 km depth is caused by ~15 MPa overpressure. At the high porosity range (35–42%), the Ekofisk chalk has a bulk modulus of about 3-8 GPa and shear modulus of 3.5–6 GPa (Røgen et al., 2005). Røgen (2002) showed that the acoustic properties of North Sea Chalk manifest isotropy. Olsen (2007) described in detail the poroelasticity of North Sea chalk. He found that the Iso-Frame model and the Marion's bounding average method (BAM) are more consistent than the self-consistent model by Berryman when both dry and water-saturated chalks are modelled. The derived poroelasticity coefficients are related to the degree of cementation and thus may also provide a proxy for Archie's cementation factor (Archie, 1942).

The studied Late- Cretaceous organic-rich chalk in the Shefela basin is situated in a syncline associated with the “Syrian Arc” folding system (Meilijson et al., 2014). This NE–SW elongated structure is about 90 km long and about 35 km wide (Fig. 1), and includes organic-rich sections with minimum thickness of 150 m (Gvirtzman et al., 1985). The sequence may be as thick as 550 m (Minster, 2009), and it constitutes the largest known organic-rich deposit in Israel, perhaps even in the Levant region. The kerogen classification is type IIS, due to its deep marine origin and high amounts of sulfur (Spiro, 1980). This thick sequence is located in the Shefela basin at shallow depths (several hundreds of meters), and was never exposed to significantly high temperatures. Consequently, the organic-rich chalk in the Shefela basin is an immature source rock. The kerogen-chalk mixture results in a high porosity, fine grained, dark brown rock, which contains mostly fine grained components (kerogen and micrite), some micron-scale foraminifers, and in some places large visible fossils and thin marl beds (Bisnovat et al., 2015; Burg et al., 2010). There are hardly any open fissures and bedding directivity is barely recognized in the naked eye. *In situ* stress measurements show that the stress field in the region is characteristic of “normal faulting” (e.g. Zoback, 2010), with maximum horizontal stress acting in ESE-WNW direction (Gersman et al., 2012).

In this study we performed laboratory measurements on cores from Zoharim well. The extensive research previously performed on Aderet well (Bisnovat et al., 2015) provides us with a good background for the mechanical and petrophysical behavior of this rock type. Enhancements obtained in the current study include ultrasonic velocities and dynamic elastic moduli, together with some modifications in the experimental methodology. Moreover, here the poroelasticity of the chalk is being thoroughly investigated, in order to improve interpretation of field tests (well logs and surface surveys), mainly regarding porosity, TOC, and fluid saturation. At this stage, the dynamic elasticity moduli of the organic-rich chalk are assumed to be isotropic, an issue we plan to further explore in the future. The main goal of this study is to obtain a deep understanding of the effects kerogen has on the physical nature of immature organic-rich chalks.

2. Methods

2.1. Petrophysical properties and ultrasonic velocities

Porosity, permeability and solids density were measured using Coreval30 poro-permeameter system, manufactured by Vinci Technologies, using Nitrogen gas. The measurements were performed on 1 inch length and 1 inch diameter oven-dried core plugs. Overall 65 samples from Ghareb formation and 24 samples from Mishash formation were measured. The plugs were subjected to 400 psi confining pressure during the tests. Geochemical analysis of the organic material focused on TOC measurements of cores, using an SC632 LECO for organic carbon and sulfur. TOC measurements were performed by Israel Energy Initiatives (IEI Ltd).

Ultrasonic velocities of core plugs, 1 inch length and 1 inch diameter, were measured using the Acoustic Velocity System

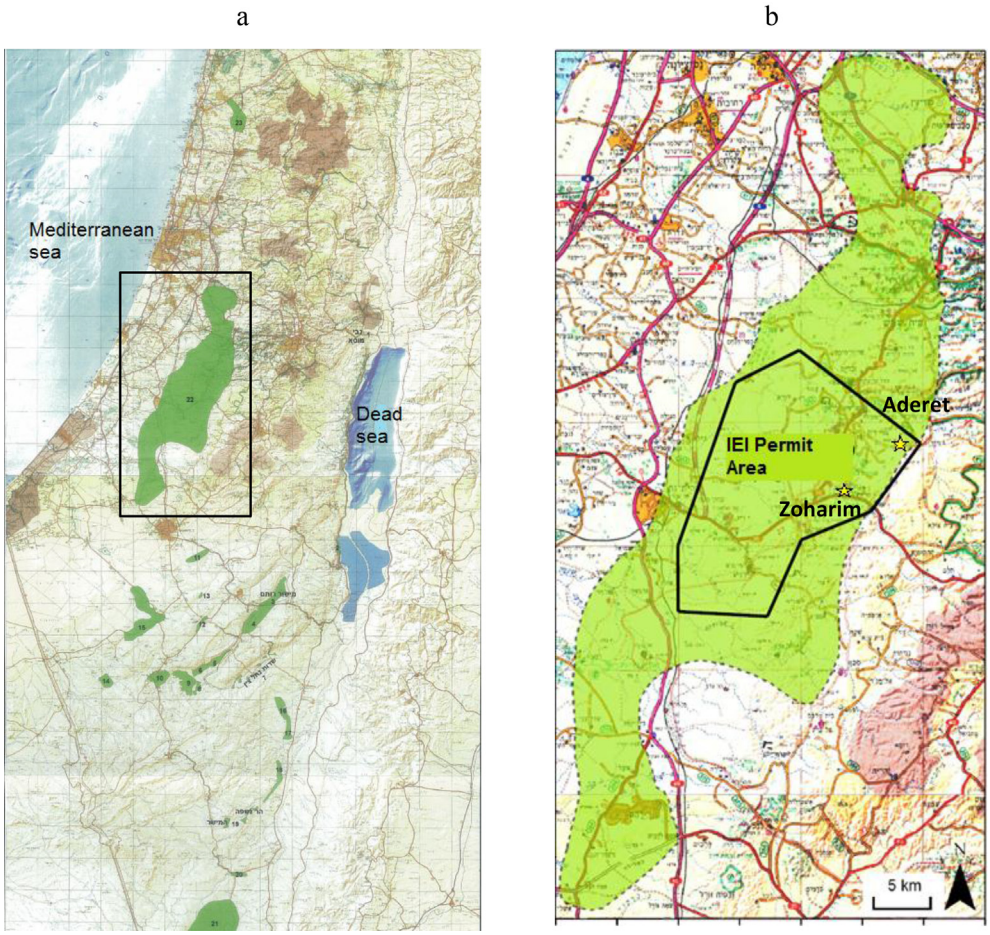

Fig. 1. Modified from Minster (2009): a) Map of organic-rich deposits (oil shales) in Israel; b) the extent of the Shefela deposit, where organic-rich sequence is > 250 m thick, including the locations of Zoharim and Aderet boreholes (marked by stars) within the permit area of IEI Ltd., (shown in the polygon).

(AVS350) manufactured by Vinci Technologies. Velocities were measured normal to the bedding direction, and dynamic elastic moduli, specifically bulk modulus K and shear modulusμ were computed, assuming isotropy, as follows:

$$K = \rho_b \left(v_p^2 - \frac{4}{3} v_s^2 \right) \quad (1)$$

$$\mu = \rho_b v_s^2 \quad (2)$$

where ρ_b is bulk density, v_p is the P wave velocity and v_s is the S wave velocity. Porosity and density data were taken from adjacent core plugs oriented parallel to the bedding direction. The AVS350 system is designed for high-frequency signals using 500 kHz piezoelectric transducers. The ultrasonic waves traverse through pressurized core plugs, with separate manual control on axial, radial, and pore pressures. The pressures applied during the tests simulated the in situ stress conditions: axial pressure simulated the vertical stresses as computed from density-log data, and radial pressures simulated the minimum horizontal stress as estimated from hydraulic fracturing tests, performed by Golder Associates. We saturated the plugs with saline water (0.6 mgNaCl/g), and induced pore pressures assuming a hydrostatic gradient from the observed level of the ground water table in the field. Tests were carried out on 52 samples from Ghareb formation and 13 samples from Mishash formation from the Zoharim well.

Well log data of density, neutron porosity, acoustic velocity, and TOC data collected during continuous coring were supplied by IEI Ltd.

2.2. Strength measurements

Indirect (Brazilian) tensile strength tests were performed using a manual, hydraulic, mini-load frame (SBEL model PLT-75). Cylindrical specimens were used, 54 mm diameter and 27 mm thickness, maintaining t/D ratio of 0.5, according to ASTM and ISRM standards. The specimens were kept at room conditions before the tests. Samples were drilled both parallel and perpendicular to the bedding direction, to allow for mechanical anisotropy. We measured tensile strengths both in the bedding-normal direction (tension applied normal to bedding direction) and the bedding-parallel direction (tension applied parallel to bedding direction).

Triaxial compression experiments were performed using a hydraulic, servo controlled testing system manufactured by TerraTek Inc., model FX-S-33090. Tests were carried out on NX size right solid cylinders with diameter of 54 mm and L/D ratio of about two. Tests were performed under constant axial strain rate of 1×10^{-5} sec^{-1}. All triaxial tests were performed with the bedding plane direction normal to the axis of the solid cylinders. Each test initiated at the confining pressure assumed to prevail at each depth, based on in situ stress measurements. In addition to compressive strength, the static elastic coefficients Young's modulus (E) and Poisson's ratio (ν) were derived from the slopes of the stress–strain curves in the linear zone, as follows:

$$E = \Delta\sigma_a/\Delta\varepsilon_a \quad (3)$$

$$\nu = -\Delta\varepsilon_r/\Delta\varepsilon_a \quad (4)$$

where σ and ε are normal stress and normal strain, respectively, and subscripts 'a' and 'r' denote axial and radial directions, respectively.

We sampled specimens for compressive and tensile strength tests from ten different depths, five from the Ghareb formation and five from the Mishash formation. The specimens were kept at room conditions before the tests in order to avoid fractures caused by drying in an oven. Following each test, the fragments of the specimen were weighed, dried in an oven and then weighed again, in order to calculate the water content ω:

$$\omega = \frac{m_w}{m_s} \quad (5)$$

where m is mass, and subscripts w and s refer to water and solid phases, respectively.

3. Experimental results

3.1. Porosity and density

Core porosity decreases consistently from ~45% at the top of the Ghareb–Mishash complex to ~23% at the bottom (Fig. 2). The decrease rate exhibits two different trends: 0.03% φ/m in the Ghareb Fm., and 0.1% φ/m in the Mishash Fm. (note that percentage is amount of porosity loss and not a relative percentile decrease). Similar porosity decrease rates are observed in Aderet well (data from Bisnovat et al., 2015), which is 7 km away from Zoharim well (Fig. 1), where the rates are 0.02% φ/m in the Ghareb Fm. and 0.07% φ/m in the Mishash Fm. The top of the Aderet sequence is shallower than Zoharim's by ~65 m, and the Ghareb–Mishash interface by ~25 m. The porosity decrease rate of the Ghareb Fm. is very similar to the rate observed in the organic-lean Niobrara chalk. Furthermore, porosity and TOC do not exhibit a clear correlation (Fig. 3), thus kerogen does not appear to occupy pore volume but to form part of the solid skeleton. This is supported also by SEM images discussed later. We conclude that kerogen has only a minor influence on the rate of compaction. The sharper porosity decrease in the Mishash Fm. may be caused by silica enrichment and increased cementation at the deep zones of the interval.

The continuous curve in Fig. 2 shows porosity obtained from the neutron well log, compared with porosity measured at the laboratory. The neutron porosity tool measures the hydrogen index (HI) of the rock unit (not to be confused with HI obtained from Rockeval pyrolysis). In immature carbonate source rocks the neutron porosity detects the HI of kerogen, in addition to the HI of the pore fluid (water). Therefore, neutron porosity is significantly higher than the core porosity, and the gap between the two datasets is mostly attributed to the kerogen. This inference is supported by the magnitude of the gap, which is larger in the kerogen-rich zone (Lower Ghareb interval).

Solids density depends almost exclusively upon the changes in TOC, as demonstrated in Fig. 4. Mass and volume balance relationships can be expressed in terms of TOC (e.g. Eq. (8) in Vernik and Nur, 1992). Accounting for dry conditions, these relationships provide the dependency of solids density on TOC:

$$\rho_s = \frac{\rho_m}{1 + \left(\frac{\left(\frac{\rho_m}{\rho_k} - 1\right)}{100C_k}\right) TOC} \quad (6)$$

where ρ_m and ρ_k are the densities of minerals and kerogen, respectively, and C_k is carbon weight fraction in the kerogen. Carbon weight percentage in the organic matter is about 70% ($C_k \sim 0.7$), as obtained from elemental analysis of kerogen in the Zoharim sequence. Consequently, the expected solids density-TOC trend line is in the form of:

$$\rho_s = \frac{a_1}{1 + a_2 TOC} \quad (7)$$

where:

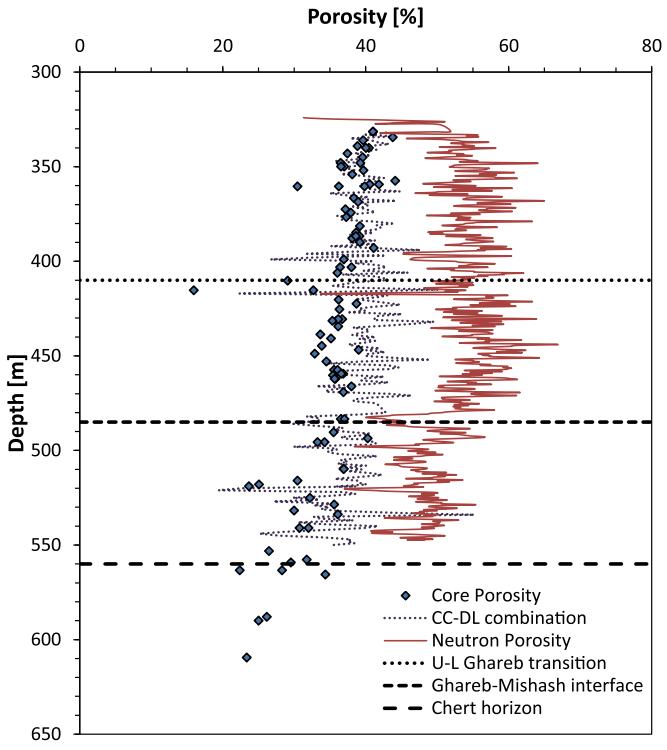

Fig. 2. Depth profile of porosity in the Zoharim well obtained by core measurements (circles), neutron log (continuous curve), and computed values obtained by combining TOC continuous coring data with density log data (dashed curve).

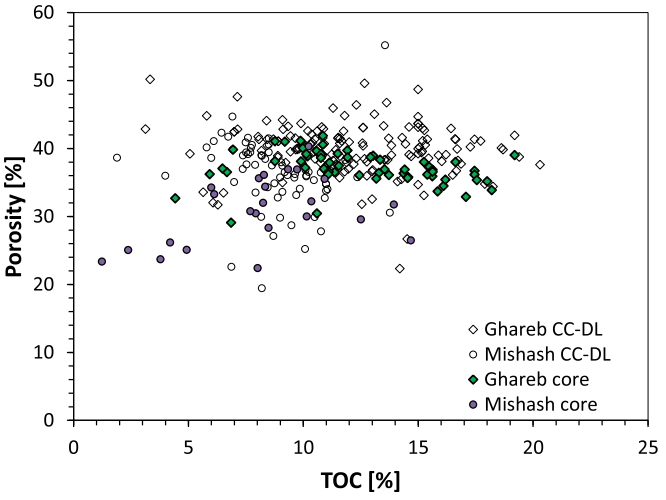

Fig. 3. Porosity and TOC in Ghareb and Mishash formations, obtained from core plugs and from continuous coring-density log (CC-DL) combination.

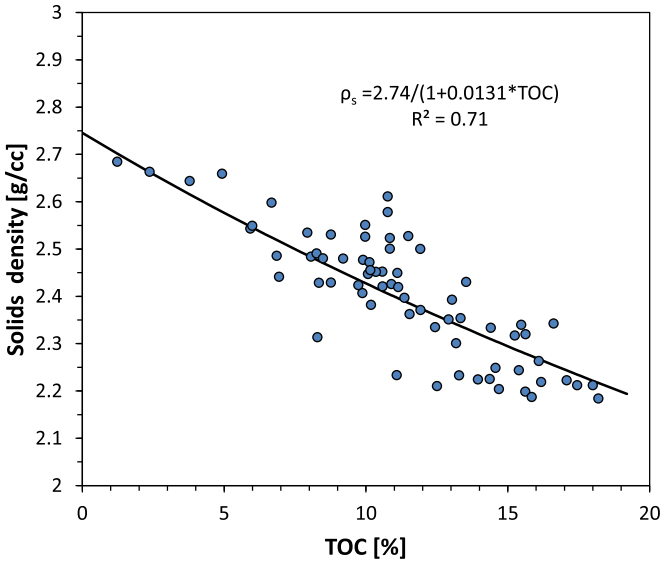

Fig. 4. Solids density measured (diamonds) and calculated from TOC data (curve).

$$a_1 = \rho_m \quad ; a_2 = \frac{\frac{\rho_m}{\rho_k} - 1}{100 C_k} \tag{8}$$

Average kerogen density is therefore derived:

$$\rho_k = \frac{\rho_m}{100 C_k a_2 + 1} \tag{9}$$

The best-fit densities of the mineralogical and organic phases represent the average densities over the entire Ghareb–Mishash complex. The results of this analysis show that minerals density averages about 2.74 g/cc, a value that is very close to the density of calcite (Mavko et al., 2009). The kerogen density is found to be 1.43 g/cc, relatively high with respect to other kinds of type II kerogen, presumably due to high sulfur concentration. Kerogen density is used for calculating its fractional volume (f_k) in each sample (modified from Vernik and Nur, 1992):

$$f_k = \frac{TOC\ \rho_{dry}}{100 C_k \rho_k} \tag{10}$$

where ρ_{dry} is the bulk density of the dry cores measured in the Coreval30 system. The volumetric fraction of the mineralogical phase is then computed:

$$f_m = 1 - \varphi - f_k \tag{11}$$

In order to generate a dense porosity dataset, we combine TOC from continuous coring data (values are spaced by 1 m) with bulk density from well-logs (values are spaced by 0.15 m):

$$\varphi = (\rho_s - \rho_b) \Big/ \left(\rho_s - \rho_f\right) \tag{12}$$

where ρ_s is solids density, computed based on TOC data and the relationship shown in Eq. (6), ρ_b is bulk density from well logs, and ρ_f is the fluid density (water). The porosity values obtained from this continuous coring-density log combination (CC-DL in Fig. 2) show an excellent match with core porosity.

3.2. Ultrasonic wave velocities

The ultrasonic velocities of P and S waves of the water-saturated chalk show no significant variations within the Ghareb and upper Mishash formations. Results are given in Table 1, and average velocities and dynamic moduli are summarized in Table 2. The elastic moduli are somewhat lower than those reported for other high porosity chalks (Japsen et al., 2004; Maldonado et al., 2011; Olsen, 2007), possibly due to the compliant nature of kerogen and the shallow depth of burial. Notably, the dynamic elastic moduli of the silica-enriched lower Mishash interval are much higher due to sharp decrease in porosity and TOC, as well as increase in silica cementation.

Measurements of P wave velocities on core plugs are in good agreement with those obtained by sonic log data within the lower part of the Ghareb Fm. and upper part of the Mishash Fm. (Fig. 5). A considerable gap between core data and log data is observed in the upper part of the Ghareb Fm. (330–400 m), below the Taqiye formation which is a thick clay-marl layer and believed to be an excellent seal against gas migration. This gap is most likely caused by the presence of gas in the shallow parts of the section, which causes P-wave velocity reduction by 100–600 m/s. This gas accumulation is encountered also in the corresponding zone in the Aderet well, based on five acoustic measurements we performed on cores from this zone. This finding motivates us to model fluid substitution and compute gas saturations. In this paper we present two fluid substitution models, the Biot-Gassmann model and Marion's BAM model, which are designed for these purposes. We examine here the applicability of the fluid substitution models and study through them the poroelasticity of the organic-rich chalk.

3.3. Compressive and tensile strength

Tensile strengths of air-dried Zoharim cores are summarized in Table 3 and shown in Fig. 6a. A general increase of tensile strength with depth is observed, but in the upper part of the Mishash Fm. the strength is somewhat constant or even decreased. Mechanical anisotropy is clearly exhibited, as the chalk is more resistant to tensional stresses acting parallel to bedding ($\sigma_{t,p} = 1.8–5\ MPa$) rather than normal to bedding ($\sigma_{t,n} = 0.5–3.5\ MPa$). The average parallel/normal strength ratio is about 1.5 (force directions are demonstrated in Fig. 6b).

Triaxial compression tests of air-dried cores are summarized in Table 3, and strengths are plotted against depth in Fig. 7. It is evident that the strength generally increases with depth, but in the upper part of the Mishash Fm. the compressive strength decreases, as observed for the tensile strength. This is most possibly a result of sampling highly porous cores from the upper part of the Mishash formation. That interpretation is based on the linear regression between both compressive strength and tensile strength with porosity, as can be seen in Fig. 8. Surprisingly, no clear dependency between strength and kerogen volume is observed (Fig. 9). The average ratio between compressive strength and tensile strength in the normal direction is about 13.5. This value exceeds the ratio of 8 suggested by Griffith's criterion (Griffith, 1921), most likely due to bedding-parallel weakness planes that cause the bedding-normal tensile strength to diminish.

Unlike the strength, the static Young's modulus shows some dependency upon the kerogen content (Fig. 10). This observation suggests that the linear relationship often observed between strength and Young's modulus (Deere and Miller, 1966), is not encountered here. This deviation highlights the unique nature of the organic-rich chalk, with respect to other rock types. It is difficult, however, to quantify the kerogen influence, and further investigation is required in this direction. Poisson's ratio averages at about $\nu = 0.21 \pm 0.04$ over the entire Ghareb–Mishash sequence; no dependency on TOC or water content is identified.

Table 1
Porosity, water-saturated bulk density, TOC and acoustic velocities of cores from Zoharim well.

Depth [m]	Porosity [%]	Density [g/cc]	TOC [%]	Pressure [MPa]			Velocities [m/s]	
				Axial	Radial	Pore	P	S
331.5	41.01	1.87	9.2	6.8	3.7	2.9	2169	1026
334.5	43.79	2.08	10.34	6.9	3.7	2.9	2375	974
336.1	39.63	1.88	9.74	6.9	3.8	2.9	2338	990
339.1	38.84	1.85	9.7	7	3.8	2.9	2232	1069
340.1	40.03	1.92	9.98	7	3.8	2.9	2660	1303
343.1	37.44	1.85	11.45	7.1	3.9	2.9	2257	1063
345	39.57	1.97	8.58	7.1	3.9	3	2495	1163
348	36.50	1.93	11.5	7.2	3.9	3	2383	944
352	39.70	1.9	11.92	7.2	3.9	3.1	2448	1119
354.1	38.11	1.91	9.59	7.3	4	3.1	2357	872
357.5	40.00	2.04	10.03	7.4	4	3.1	2416	965
359.4	40.57	2.04	10.85	7.4	4	3.1	2297	1154
360.5	39.83	1.87	6.94	7.4	4	3.1	2429	1060
366.6	38.34	1.83	13.4	7.5	4	3.2	2397	955
366.6	38.34	1.83	13.4	7.5	4	3.2	2129	913
374.5	37.91	1.88	10.72	7.6	4.1	3.3	2447	960
376.7	37.28	1.84	13.57	7.7	4.1	3.3	2288	998
381.5	39.17	1.9	9.7	7.6	4.1	3.3	2440	965
384.8	38.67	1.84	11.3	7.8	4.1	3.4	2307	972
386.8	40.55	1.99	10.77	7.9	4.2	3.4	2462	1219
387.9	38.13	1.95	8.51	7.9	4.2	3.4	2331	1107
393	41.13	1.83	10.87	8	4.2	3.4	2362	1053
399.1	36.93	1.9	13.54	8.1	4.2	3.5	2442	1028
403.2	36.40	1.78	16.62	8.2	4.3	3.6	2256	971
406.2	36.05	1.85	13.17	8.2	4.3	3.6	2266	1133
410	29.08	2.05	8.29	8.2	4.3	3.6	2242	990
415.4	32.67	1.87	4.43	8.4	4.3	3.7	2551	1048
420.5	36.22	1.79	15.67	8.4	4.3	3.7	2329	1134
422.5	38.72	1.83	12.83	8.5	4.4	3.7	2525	1186
425.5	36.33	1.78	15.14	8.5	4.4	3.8	2466	1129
429.5	36.00	1.78	18.02	8.6	4.4	3.8	2228	1024
430.6	36.14	1.76	17.45	8.6	4.4	3.8	2396	1160
434.5	36.15	1.79	15.42	8.7	4.4	3.9	2284	1117
438.7	33.67	1.79	16.34	8.8	4.5	3.9	2409	1166
440.8	35.16	1.79	16.53	8.8	4.5	3.9	2433	1188
444.8	33.85	1.78	17.55	8.9	4.8	4	2415	1180
446.9	39.00	1.75	19.2	8.9	4.9	4	2307	1118
448.9	32.88	1.82	17.08	8.9	5	4	2592	1192
453	34.49	1.83	16.24	9	5	4	2249	1110
460.3	35.41	1.79	15.5	9.1	5.1	4.1	2288	1004
462.1	35.65	1.81	14.54	9.2	5.1	4.1	2553	1053
469.2	36.88	1.84	13.91	9.3	5.2	4.2	2267	1097
483.5	37.04	2.01	6.48	9.5	5.3	4.3	2339	1142
489.5	35.51	1.94	10.93	9.7	5.3	4.4	2215	1067
493.6	40.29	1.84	10.24	9.7	5.3	4.4	2462	1044
495.7	33.26	2.01	6.13	9.8	5.4	4.5	2822	1124
498.7	35.00	1.91	8.17	9.8	5.4	4.5	2369	1016
516	30.45	2.06	7.86	9.9	5.5	4.6	2516	1072
518	25.08	2.24	4.08	10.2	5.8	4.7	2572	1062
525.1	32.19	1.98	9.29	10.3	5.9	4.8	2537	1202
533.8	36.10	1.84	13.92	10.5	6.1	4.8	2492	1128
553.2	26.46	1.89	13.49	10.9	6.5	5	2780	1325
557.8	31.74	1.84	13.86	11	6.5	5	2232	992
559.3	29.50	1.85	13.68	11	6.6	5.1	2356	967
565.6	34.35	1.93	7.51	11.1	6.9	5.1	2606	1258
588	26.11	2.18	4.2	11.6	7.1	5.4	3467	2001
590	25.03	2.25	2.38	11.6	7.1	5.4	3683	1970
609.5	23.35	2.29	1.38	12.1	7.5	5.6	3519	1949

Table 2
Average acoustic properties of organic-rich chalk in Zoharim borehole.

Interval	P-wave velocity [km/s]	S-wave velocity [km/s]	Poisson's ratio	Young's modulus [GPa]	Bulk modulus [GPa]	Shear modulus [GPa]
Ghareb- Upper Mishash	2.38 ± 0.17	1.07 ± 0.09	0.37 ± 0.03	5.9 ± 1	7.8 ± 1.5	2.2 ± 0.4
Lower Mishash	3.56 ± 0.11	1.97 ± 0.03	0.28 ± 0.02	22.3 ± 0.4	16.7 ± 2.1	8.7 ± 0.0

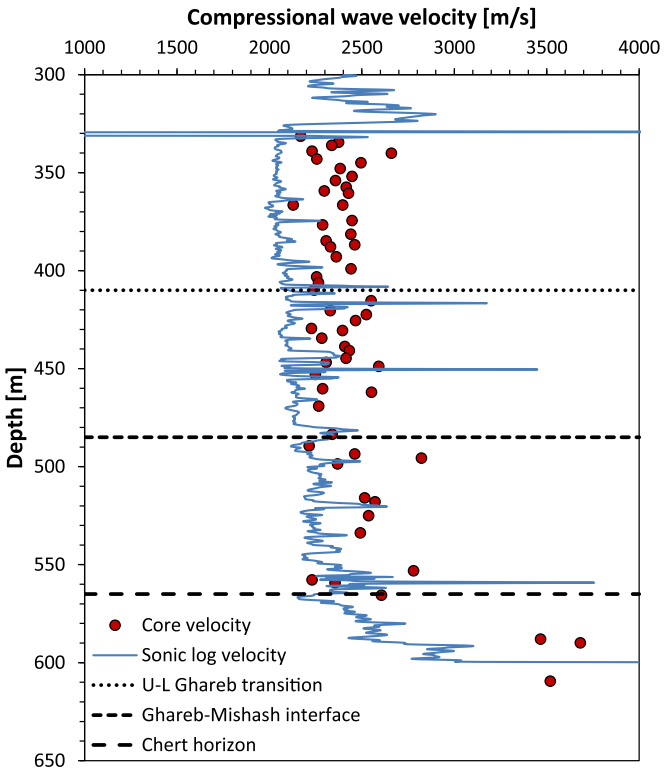

Fig. 5. Core-log data comparison of P wave velocity.

(Fig. 11b), although a better convergence of K_{sat} around an apparent trend is obtained when the volume fraction of both kerogen and pores is considered (Fig. 11c). This may imply that it is the volumetric fraction of the minerals (f_m) that dictates the stiffness of the chalk under dynamic loading conditions, whereas the kerogen contributes very little to chalk incompressibility.

In addition to the relative concentration of the constituents, the bulk modulus also depends on the geometrical arrangement of them within the rock, which influences the pores stiffness (Mavko et al., 2009). Pore stiffness relates to mechanical interactions at the contacts between stiff and soft grains within a porous medium. For example, stiff pore geometry may be encountered where the stiff phase (here calcite) constitutes a well-connected frame, with little interference of the soft grains (here kerogen).

Elastic moduli of multiphase materials are calculated using the Hashin-Shtrikman (HS) bounds (Hashin and Shtrikman, 1963). The upper and lower bounds represent the stiffest and softest pore geometries, respectively:

$$K_{HS}^{+} = \left(\sum_{i=1}^{n} \frac{f_i}{K_i + \left(\frac{4}{3}\,\mu_{max} \right)} \right)^{-1} - \frac{4}{3}\mu_{max} \tag{13}$$

$$K_{HS}^{-} = \left(\sum_{i=1}^{n} \frac{f_i}{K_i + \left(\frac{4}{3}\,\mu_{min} \right)} \right)^{-1} - \frac{4}{3}\mu_{min} \tag{14}$$

Table 3
Strength results from compression and tension tests. Starred porosity values are estimated from continuous coring-well log data combination and adjacent core data, where exact core data is missing.

Depth [m]	Porosity [%]	TOC [%]	Dry bulk density [g/cc]	Triaxial compression test			Brazilian test	
				Confining pressure [MPa]	Peak stress difference [MPa]	Young's modulus [GPa]	Bedding normal tensile strength [MPa]	Bedding parallel tensile strength [MPa]
339.1	38.84	10.31	1.43	3.65	9.78	1.72	0.48	2.16
360.5	38.00	9.74	1.47	4.55	17.8	1.63	1.75	2.66
388.9	38.65	10.2	1.52	6.37	19.7	–	1.32	3.13
431.5	35.92	17.72	1.38	4.9	29.2	2.14	2.41	3.69
457.5	35.57	14.6	1.45	6	31.23	2.57	2.37	3.99
517	38.7*	8.18	1.84	5.86	17.4	2.12	2.00	1.81
540	35.65*	6.74	1.68	5.6	28	3.68	2.26	3.04
559.3	29.54	13.68	1.54	6.37	42.4	2.39	2.92	5.75
588	26.15	4.21	1.92	6.77	49.66	5.36	3.72	5.24
609.5	23.35	1.3	2.03	7.54	52.8	8.28	3.53	3.89

4. Discussion

4.1. Poroelasticity

Our goal is to understand the mechanisms that determine the dynamic mechanical behavior of the rock, specifically the bulk modulus (K). In order to do so, we use poroelasticity theories to describe the features of this three-phase medium. Volumetric fractions of minerals, kerogen and pores are derived from the measurements of porosity, density and TOC. Modelling is based on the computed volumes (Eq. (10) and (11)) and theoretical moduli of the phases (Table 4).

The bulk modulus typically depends on the relative concentrations of the rock constituents. Here we treat the kerogen as a matrix constituent; not as pore fill but rather as skeletal material. Our results indicate that the bulk modulus of the saturated rock (K_{sat}) is dependent upon the porosity (Fig. 11a) and the kerogen content

where K_{HS}^{+} and K_{HS}^{-} are upper and lower HS bounds, respectively, and μ_{max} and μ_{min} are the shear moduli of the phases with the highest and lowest shear moduli, respectively. The calculations are made using the theoretical modulus of each phase (K_i) and its individual volume (f_i). We use the relationships shown in Eqs. (10) and (11) in order to adjust this model to organic-rich source rocks which are approximately isotropic:

$$K_{HS}^{+/-} = \left(\frac{\varphi}{K_f + \frac{4}{3}\mu_{m/f}} + \frac{\frac{\rho_{dry}}{\rho_k}\frac{TOC}{100C_k}}{K_k + \frac{4}{3}\mu_{m/f}} + \frac{\left(1 - \varphi - \frac{\rho_{dry}}{\rho_k}\frac{TOC}{100C_k}\right)}{K_m + \frac{4}{3}\mu_{m/f}} \right)^{-1} - \frac{4}{3}\mu_{m/f} \tag{15}$$

where subscripts 'f', 'm' and 'k' denote fluid, minerals and kerogen,

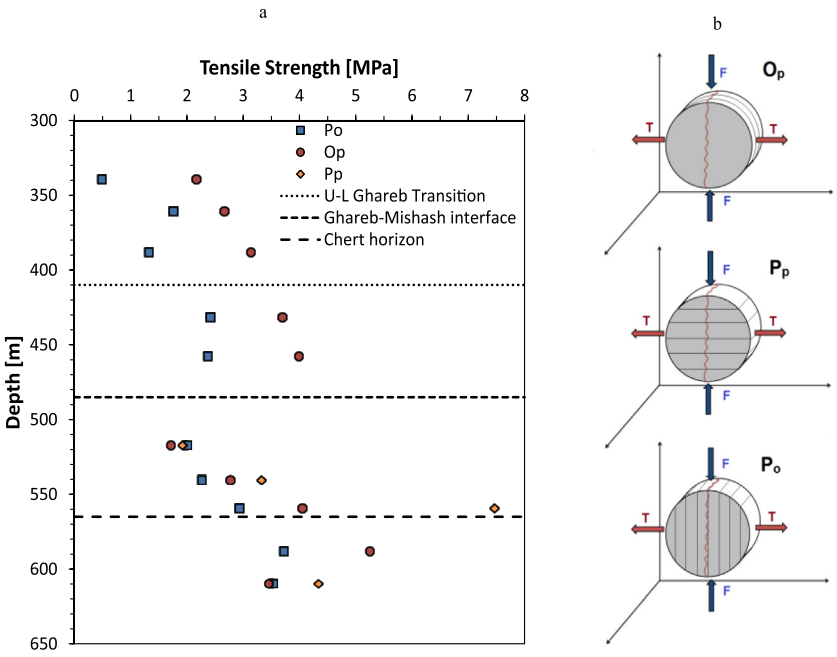

Fig. 6. a) Vertical tensile strength (crosses) and horizontal tensile strength (circles) plotted vs. depth in the Zoharim well; b) three different orientations tested, where O_p and P_p represent the horizontal strength, and P_o represents the vertical strength.

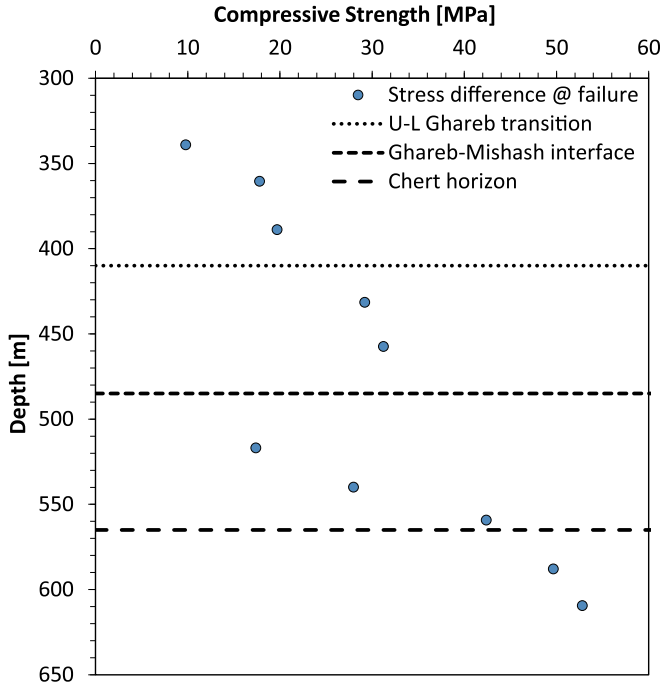

Fig. 7. Peak stress difference plotted vs. depth in the Zoharim well, confining pressures are given in Table 3.

respectively. Bulk and shear moduli of the mineralogical components are taken from the literature (Mavko et al., 2009; Wang et al., 1998). The average moduli of the minerals are calculated based on the concentration of each mineral, as obtained by X-Ray Diffraction (Table 4). Elastic properties of immature type II kerogen are reported in a few publications (Carcione, 2001; Yan and Han, 2013), while no data are available on the properties of type IIS kerogen. We take bulk modulus of kerogen $K_k = 5\ GPa$ due to the high density and immaturity of the kerogen, and shear modulus of about half the bulk modulus (Yan and Han, 2013). We study two fluid substitution models in order to compute the saturated bulk modulus of the chalk: Biot-Gassmann's method and Marion's bounding average method (BAM). By fitting model results to the experimental data we derive the poroelasticity coefficients of the chalk.

The Biot-Gassmann method is typically applicable when using seismic frequencies, where the induced pore pressure is equilibrated throughout the pore space (i.e. there is sufficient time for the pore fluid to flow and eliminate wave-induced pore-pressure gradients). The bulk modulus of the entire rock is given by:

$$K_{sat} = K_s(1-\beta) + \frac{\beta^2 K_s K_f}{K_f(\beta-\varphi) - K_s\varphi} \tag{16}$$

$$K_{dry} = K_s(1-\beta) \tag{17}$$

where subscripts *sat*, *dry* and *s* refer to the bulk modulus of saturated rock, dry rock and solid phase, respectively. The Biot's coefficient (β) determined for bulk modulus, is a dimensionless coefficient ranging from 0 to 1, and also known as the effective stress coefficient (Mavko et al., 2009; Zoback, 2010):

$$\sigma' = \sigma - \beta P_p \tag{18}$$

where σ' is the effective stress, σ is the total stress, and P_p is the pore fluid pressure.

From comparisons we made between measurements of water-saturated bulk modulus and of dry bulk modulus, the best-fit solids effective modulus (K_s) appears to be the Voigt-Reuss-Hill (VRH) average (Mavko et al., 2009):

$$K_{s,VRH} = \frac{\left(\sum_{i=1}^{n} \frac{f_i}{K_i(1-\varphi)}\right)^{-1} + \sum_{i=1}^{n} \frac{f_i}{1-\varphi} K_i}{2} \tag{19}$$

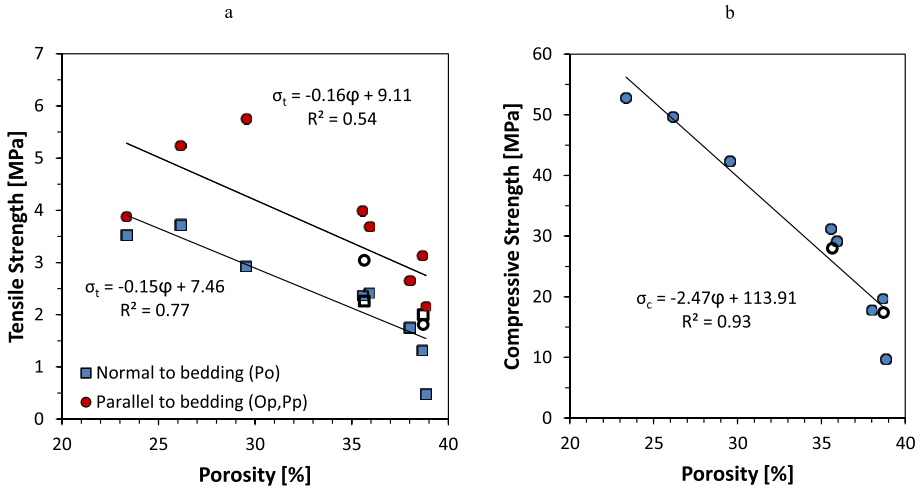

Fig. 8. Vertical tensile strength (circles in (a)), horizontal tensile strength (crosses in (a)), and compressive strength (b) show decrease linearly with porosity. Symbols in bold represent porosity calculated according to Eqs. (12) and (6), due to missing core porosity data.

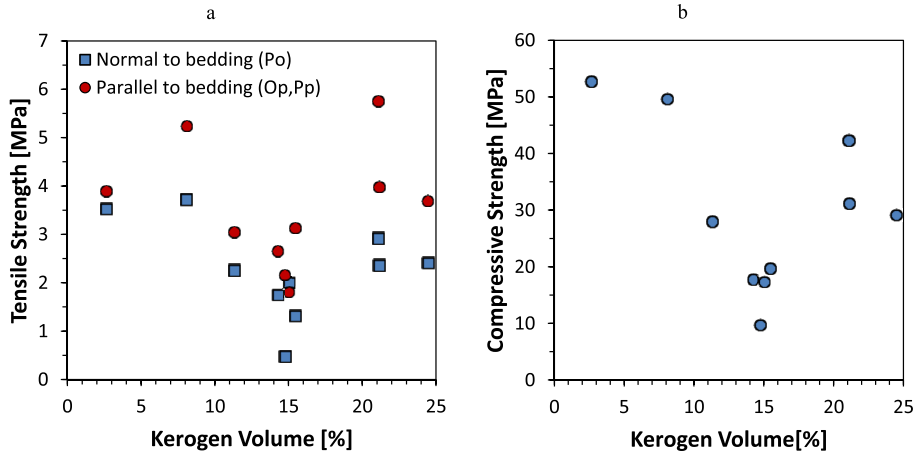

Fig. 9. Vertical tensile strength (circles in (a)), horizontal tensile strength (crosses in (a)), and compressive strength (b) show weak or no relationship with kerogen volume.

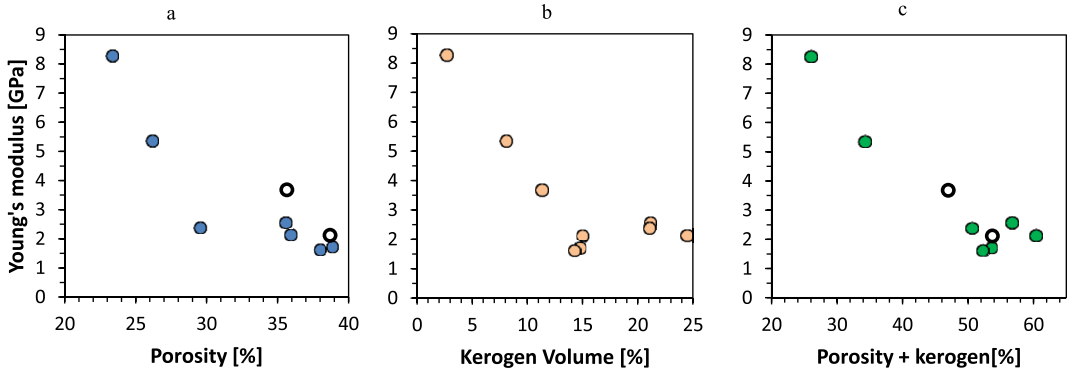

Fig. 10. Static Young's modulus regression against porosity (a), kerogen volume (b) and the sum of them.

Marion's bounding average method (BAM) argues that the vertical position between the experimental value and the theoretical Hashin-Shtrikman bounds is a measure of the pore geometry, and is independent of the pore fluid (Marion, 1990). This characteristic is defined by the normalized stiffness factor w:

$$w = \frac{K_{sat} - K^{-}_{sat,HS}}{K^{+}_{sat,HS} - K^{-}_{sat,HS}} \tag{20}$$

The normalized stiffness factor ranges between 0 and 1, where the bulk modulus coincides with the lower and the upper bound, respectively. Yan and Han (2011) validated that the difference

Table 4
Average minerals distribution and individual bulk modulus (K) and shear modulus (μ) of each phase. Minerals average volumetric concentrations (%v) are provided by IEI Ltd.

Mineral	%v	K [GPa]	μ [GPa]
Kaolinite	1	1.5	1.4
Illite	1	48	22
Smectite	7	9.3	6.9
Calcite	60	71	30
Dolomite	1	80	48
Quartz	4	37	45
K-spar	1	37.5	15
Plag	1	75.6	25.6
Pyrite	1	147	132
Apatite	23	85	54
Minerals average		59	38
Kerogen		5	2.5
Brine		2.32	0

porosity. To explore these expected trends, the poroelasticity coefficients are determined here discretely for each measured core using our analytical derivation and experimental results. It should be noted that the normalized stiffness factor (of BAM) has been very rarely discussed and documented, although we expect it to increase with depth, most likely due to cementation and/or pressure solution.

The relationship between the two poroelasticity coefficients as obtained by us is shown in Fig. 13, where a 2nd order polynomial is fitted to the data (as in Olsen, 2007). According to the principles discussed above, we see a general trend of pore stiffening in the Mishash formation (Fig. 14), although there are some abnormally stiff samples within the upper Ghareb. It can be seen that pore-stiffness is generally reduced in the organic-rich lower Ghareb interval. The upper Mishash part is a bit stiffer than the upper Ghareb part, despite the similarity in organic richness. It is therefore

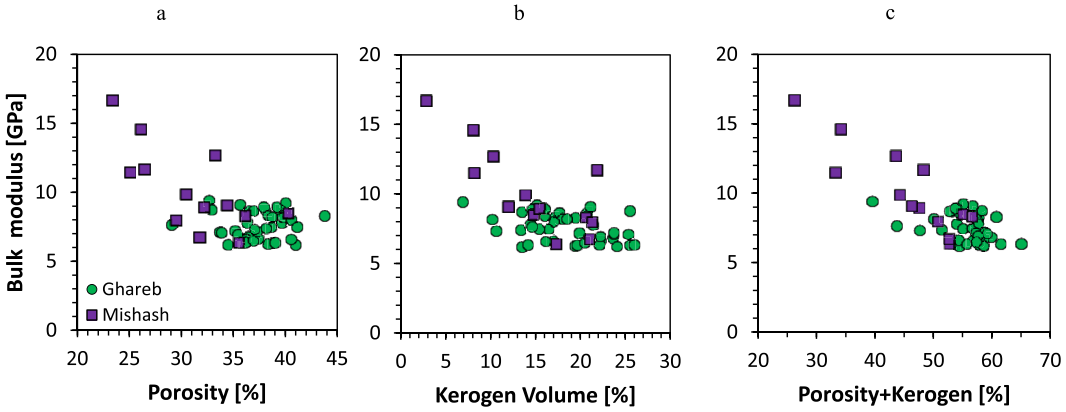

Fig. 11. Results from Ghareb Fm. (circles) and Mishash Fm. (diamonds): saturated bulk modulus (K_{sat}) vs. fractional volume of porosity (a), kerogen (b) and the sum of them (c).

between the w in dry and water-saturated conditions is negligibly small, thus it is reasonable to use this approach for fluid substitution modelling.

Both models yield fair to good correlation with the measured values of the water-saturated bulk modulus (Fig. 12). BAM results show that the best fit to the experimental data is obtained with $w = 0.21$ ($R^2 = 0.64$). Biot-Gassmann model results are best-correlated with the measured bulk modulus when using Biot's coefficient of $\beta = 0.87$ ($R^2 = 0.58$). These values are the best-fit coefficients for the entire Ghareb–Mishash sequence. The poroelasticity coefficients derived from both models indicate that the organic-rich chalk is an appreciably soft rock, whereas the measured values are close to the lower HS bound (expressed by the low normalized stiffness factor). The average Biot coefficient obtained here also indicates the chalk softness, being appreciably high with respect to other rock types (e.g. Table 4 in Detournay and Cheng, 1993). BAM predictions appear to be slightly more accurate than Biot-Gassmann in our case, and therefore more suitable for fluid substitution modelling here.

The values presented above are recommended for rock-physics modelling of the Ghareb–Mishash complex. By tracking the variations of these coefficients with depth we can track pore-stiffness variations, which may explain the porosity decrease with depth. It is typically assumed that during compaction porosity decreases, but β remains close to unity, as compaction only rearranges the grains relative to each other (Alam et al., 2010). Pore-stiffening is assumed to be caused by contact cementation among other mechanisms, and consequently β declines, independently of

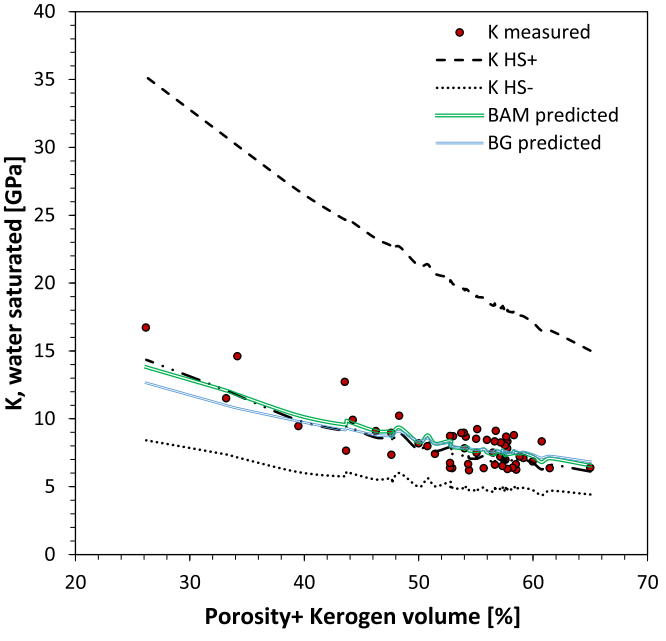

Fig. 12. Saturated bulk modulus vs. the sum of kerogen and pores volumetric fractions: measured results plot between upper and lower Hashin-Shtrikman bounds. Best-fit of BAM and Biot-Gassman models are also shown in continuous curves.

concluded that the pore stiffness is influenced by both the degree of

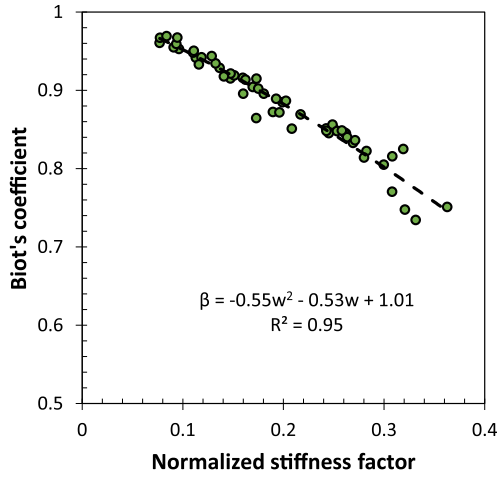

Fig. 13. Relationship between Biot's coefficient and BAM normalized stiffness factor.

where elongated particles (mainly detrital particles) tend to orient horizontally when first precipitated due to the gravity. Most of the pores are inter-particle rather than intra-particle, the amount of inter-particle pores is very large, and that causes the softness that is typical to chalks. Pore size is within the micropore -nanopore range (Loucks et al., 2012), but the pores within the kerogen are not visible thus kerogen intra-particle porosity is within the nanopore-picopore range. Kerogen is identified as cumulates that tend to align in parallel to the bedding direction (Fig. 15b), also marking bedding directivity. As claimed before, we suggest that the kerogen constitutes part of the solid skeleton, and that is evident by the scattered distribution of the kerogen in the matrix. That distribution is believed to interfere with the continuity of the mineralogical network, thus the organic-rich chalk is softer than non-organic chalks. It can be further deduced that the mixture of kerogen and microcrystalline calcite particles constitute the load supporting matrix of the chalk.

The main differences between the samples from the Ghareb

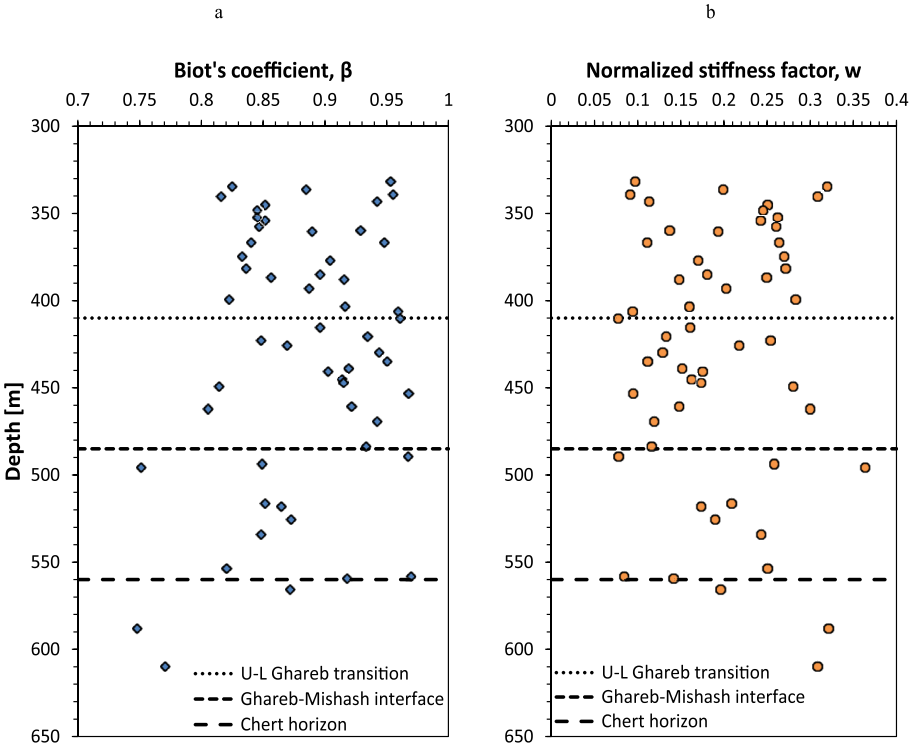

Fig. 14. Depth profiles of the poroelasticity coefficients β (a) and w (b), in the Zoharim well.

cementation as well as the kerogen content.

4.2. Microstructure from SEM

A sample taken from 430.6 m depth (lower part of the Ghareb formation) was scanned in SEM (Fig. 15). This sample is very rich in organic matter (TOC = 17.45%), porosity is 36.5%, and minerals constitute only ~39% of the rock volume. Another sample, taken from 553.2 m depth (upper part of the Mishash formation) was scanned in SEM (Fig. 16). This sample contains a little less organic matter (TOC = 13.49%), and is much less porous (φ = 26.5%). In both backscatter SEM images (Fig. 15a) we notice the bedding directivity, which is prominent only at the 10–1000 μm scale. Bedding directivity is assumed to be caused by initial depositional environment, formation (Fig. 15) and from the Mishash formation (Fig. 16) are the skeleton stiffness and the porosity. This may be due to size of the calcareous aggregates that 'float' in the matrix. The aggregates in the Mishash sample are coarser than in the Ghareb sample, and that may cause the increased mineralogical abundance that also increases material stiffness in that zone. No difference in kerogen texture can be observed in the SEM images, and in order to study processes that occur within the kerogen intra-particle porosity higher resolution tools are required. The postulated mechanisms for porosity decrease with depth that we suggested before (kerogen contents, cementation, silica enrichment) can be implied from the scans, but stronger conclusions require further investigation.

Inspection of SEM micrographs reveals that the kerogen cumulates are dispersed within the matrix rather than located in

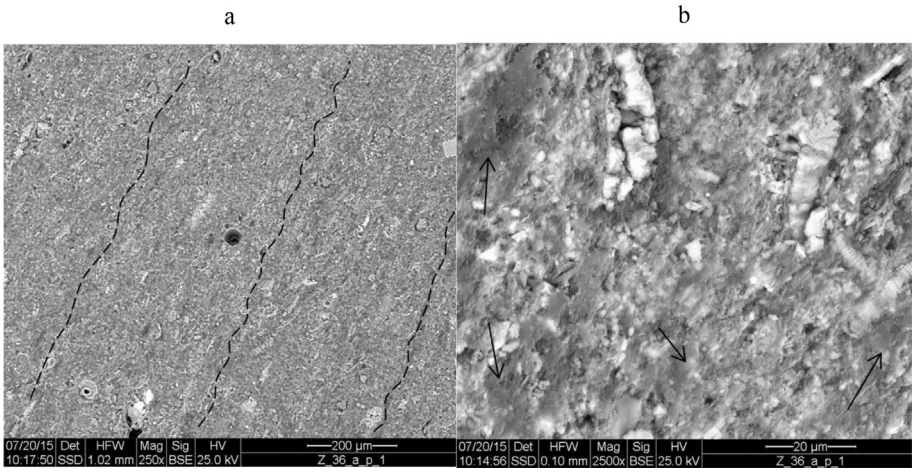

Fig. 15. SEM images of core from 430.6 m depth (lower part of the Ghareb formation). Properties: $\varphi = 0.364$, $k_h = 0.1$ **mD**, $k_h/k_v = 2.9$, $f_k = 0.244$, $f_m = 0.391$, $\beta = 0.95$, $w = 0.12$. Bedding directions are marked by dashed lines in (a) and kerogen aggregates are marked by arrows in (b).

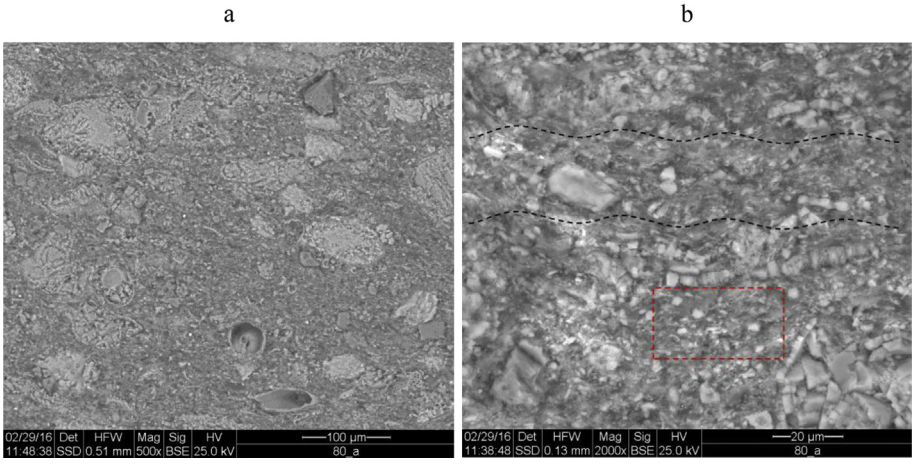

Fig. 16. SEM images of core from 553.2 m depth (upper part of the Mishash formation). Properties: $\varphi = 0.265$, $k_h = 0.02$ **mD**, $f_k = 0.218$, $f_m = 0.517$, $\beta = 0.82$, $w = 0.25$. Bedding directivity is hardly recognized in (a), and better recognized in (b). Dashed rectangle in (b) marks a matrix-representative zone which mainly contains kerogen microcrystalline calcite, with some quartz and apatite.

layers, and by that differ from organic-rich shales, which typically exhibit a laminated structure (Carcione et al., 2011; Vernik and Nur, 1992). As a result, the degree of anisotropy in organic-rich chalks is lower than in organic-rich shales. Kerogen morphology frequently exhibits some elongation in parallel with bedding direction. That can be caused by deformation due to the lithostatic overburden, and by the original orientation when first deposited. Røgen (2002) showed that the North Sea chalks (Ekofisk, Ekofisk tight, Tor and Tuxen Formations), which do not include organic matter, exhibit velocity isotropy of P and S waves over a wide range of porosities (20–50%). Hence, we can conclude that the mineralogical matrix of the organic-rich chalk can also be approximated as isotropic. By recalling that kerogen is also assumed to be isotropic, we infer that the minerals–kerogen complex is nearly isotropic (Carcione et al., 2011), and we have preliminary acoustic velocity data to support this (Gordin et al., 2016). The transverse isotropy seen in tensile strength (Fig. 6) is explained by bedding-parallel microcracks and the preferred orientation of elongated particles. Probing into acoustic anisotropy and stress sensitivity in this rock are planned for future research.

5. Summary and conclusions

We investigate the rock physics of thermally immature kerogen-rich chalk from the Shefela basin, based on core and well log data. Kerogen effects are at the focus of this paper. The most important development provided here is the poroelasticity model for the organic-rich chalk, which is examined with respect to non-organic chalks and organic-rich shales. As expected, the organic-rich chalk exhibits a relatively soft pore-geometry, characterized by low values of the normalized stiffness factor and high values of Biot's coefficient. We observe that both values are influenced by kerogen content, but it is assumed that these are controlled also by the grain size and degree of cementation. This is in agreement with matrix appearance in SEM images. The lower porosity in the Mishash formation is caused by compaction, cementation, coarser grains and silica enrichment in this zone. The poroelasticity models proposed here are derived assuming isotropy, and found to be sufficient for fluid substitution modelling. Comparison between acoustic velocities measured on core samples and sonic well log data detects gas in the upper Ghareb interval. The model we show here simplifies estimation of gas saturation in this zone.

We obtain relationships between kerogen and physical

parameters such as density, acoustic velocity, bulk modulus and Young's modulus. On the other hand, it appears that the kerogen influence on porosity, compressive or tensile strengths, is minor or even non-existent. Kerogen density is relatively high due to high sulfur contents. The water-saturated bulk modulus of the chalk is reduced upon increasing volume of porosity and kerogen. Kerogen seems to have influence also on the static Young's modulus of the chalk, although the magnitude of its effect needs to be further investigated.

Mechanical strength of the organic-rich chalk is similar, but somewhat lower, than in chalks with no or negligible organic matter content of the same porosity. Both compressive strength and tensile strength depend on the porosity of specimen. Horizontal tensile strength is higher by a factor of ~1.5 than the vertical tensile strength, due to preliminary bedding-parallel discontinuities.

Acknowledgements

This research was funded by Israel Energy Initiatives, Ltd. (IEI) through BGU contract No. 87244811. We thank IEI scientists Dr. Yoav O. Rosenberg, Dr. Itay J. Reznik and Dr. Scott V. Nguyen for fruitful discussions and for joyful cooperation. We thank Leonardo Freitas and Edna Danon for TOC measurements and their great assistance in sample preparation. The senior author thanks Israel Ministry of Infrastructures, Energy and Water Resources for a fellowship awarded to graduate students performing research in petroleum geosciences. Roxana Golan from the Microscopy Unit, Ilse Katz Institute for Nanoscale Science and Technology, Ben-Gurion University of the Negev, is thanked for the assistance in scanning the samples in SEM.

References

Alam, M.M., Borre, M.K., Fabricius, I.L., Hedegaard, K., Røgen, B., Hossain, Z., Krogsbøll, A.S., 2010. Biot's coefficient as an indicator of strength and porosity reduction: Calcareous sediments from kerguelen plateau. J. Petrol. Sci. Eng. 70 (3), 282–297.

Archie, G.E., 1942. The electrical resistivity log as an aid in determining some reservoir characteristics. Trans. AIME 146 (01), 54–62.

Bisnovat, K., Hatzor, Y.H., Vinegar, H.J., Nguyen, S.V., Palchik, V., Feinstein, S., 2015. Mechanical and petrophysical behavior of organic-rich chalk from the judea plains, israel. Mar. Petrol. Geol. 64, 152–164.

Brown, R.J., Korringa, J., 1975. On the dependence of the elastic properties of a porous rock on the compressibility of the pore fluid. Geophysics 40 (4), 608–616.

Burg, A., Gersman, R., Bartov, Y., Dror, Y., Rozenthal, A., 2010. Summary Report of Beit-guvrin & Aderet Survey Wells Hydro-geological Findings. No. IEI/1/2010. IEI Ltd, Jerusalem.

Carcione, J.M., 2001. AVO effects of a hydrocarbon source-rock layer. Geophysics 66 (2), 419–427.

Carcione, J.M., 2000. A model for seismic velocity and attenuation in petroleum source rocks. Geophysics 65 (4), 1080–1092.

Carcione, J.M., Helle, H.B., Avseth, P., 2011. Source-rock seismic-velocity models: Gassmann versus backus. Geophysics 76 (5), N37–N45.

Deere, D.U., Miller, R., 1966. Engineering Classification and Index Properties for Intact Rock.

Detournay, E., Cheng, A.H., 1993. Fundamentals of Poroelasticity.

Gassmann, F., 1951. Elasticity of porous media. Vierteljahr. Naturforschenden Gesselschaft 96, 1–23.

Gersman, R., Bartov, Y., Rozenthal, A., 2012. Summary Report of Zoharim Survey Well Hydro-geological Findings. No. IEI/3/2012. IEI Ltd, Jerusalem.

Gordin, Y., Hatzor, Y.H., Vinegar, H.J., 2016. Ultrasonic velocity and anisotropy of kerogen-rich chalks. In: Israel Geological Society (IGS) Annual Meeting, Eilat, Israel.

Griffith, A.A., 1921. The phenomena of rupture and flow in solids. Philos. Trans. R. Soc. Lond. Ser. A Contain. Pap. Math. Phys. Character 221, 163–198.

Gvirtzman, G., Moshkovitz, S., Reiss, Z., 1985. Senonian to early eocene mount scopus group in the HaShefela region, central israel: Stratigraphy and basin evolution. Isr. J. Earth-Sciences 34 (4), 172–192.

Hashin, Z., Shtrikman, S., 1963. A variational approach to the theory of the elastic behaviour of multiphase materials. J. Mech. Phys. Solids 11 (2), 127–140.

Japsen, P., Bruun, A., Fabricius, I.L., Rasmussen, R., Vejbæk, O.V., Pedersen, J.M., Høier, C., 2004. Influence of porosity and pore fluid on acoustic properties of chalk: AVO response from oil, south arne field, north sea. Pet. Geosci. 10 (4), 319–330.

Korsnes, R., Wersland, E., Austad, T., Madland, M., 2008. Anisotropy in chalk studied by rock mechanics. J. Petrol. Sci. Eng. 62 (1), 28–35.

Krief, M., Garat, J., Stellingwerf, J., Ventre, J., 1990. A petrophysical interpretation using the velocities of P and S waves (full-waveform sonic). Log Analyst 31 (06).

Lockridge, J., Pollastro, R., 1988. Shallow upper cretaceous niobrara gas fields in the eastern denver basin. In: Goolsby, S., Longman, M. (Eds.), Occurrence and Petrophysical Properties of Carbonate Reservoirs in the Rocky Mountain Region. Rocky Mountain Association of Geologists, Denver, pp. 63–74.

Loucks, R.G., Reed, R.M., Ruppel, S.C., Hammes, U., 2012. Spectrum of pore types and networks in mudrocks and a descriptive classification for matrix-related mudrock pores. AAPG Bull. 96 (6), 1071–1098.

Maldonado, A., Batzle, M., Sonnenberg, S., 2011. Mechanical properties of the niobrara formation. In: AAPG Rocky Mountain Section Meeting, Cheyenne, Wyoming, USA.

Marion, D.P., 1990. Acoustical, Mechanical, and Transport Properties of Sediments and Granular Materials.

Mavko, G., Mukerji, T., Dvorkin, J., 2009. The Rock Physics Handbook: Tools for Seismic Analysis of Porous Media. Cambridge university press.

Meilijson, A., Ashckenazi-Polivoda, S., Ron-Yankovich, L., Illner, P., Alsenz, H., Speijer, R.P., Püttmann, W., 2014. Chronostratigraphy of the upper cretaceous high productivity sequence of the southern tethys, israel. Cretac. Res. 50, 187–213.

Minster, T., 2009. Oil Shale Deposits in Israel. No. GSI/18/2009. GSI, Jerusalem, Israel.

Olsen, C., 2007. Elastic and Electric Properties of North Sea Chalk. Ph.D. Thesis. Technical University of Denmark, Department of Civil Engineering, Arctic Technology Centre, ARTEK, Lyngby, Denmark.

Pinna, G., Carcione, J.M., Poletto, F., 2011. Kerogen to oil conversion in source rocks. pore-pressure build-up and effects on seismic velocities. J. Appl. Geophys. 74 (4), 229–235.

Rice, D., 1986. Relation of hydrocarbon type to maturity of organic matter in upper cretaceous chalks. In: Mumpton, F. (Ed.), Studies in Diagenesis. U.S.G.S, Denver, pp. 76–81. U.S. geological survey bulletin 1578.

Røgen, B., 2002. North sea Chalk-textural, Petrophysical and Acoustic Properties. Ph. D. thesis. Technical University of DenmarkDanmarks Tekniske Universitet, Department of Environmental EngineeringInstitut for Vand og Miljøteknologi.

Røgen, B., Fabricius, I.L., Japsen, P., Høier, C., Mavko, G., Pedersen, J.M., 2005. Ultrasonic velocities of north sea chalk samples: influence of porosity, fluid content and texture. Geophys. Prospect. 53 (4), 481–496.

Sayers, C.M., 2013. The effect of kerogen on the elastic anisotropy of organic-rich shales. Geophysics 78 (2), D65–D74.

Spiro, B., 1980. Geochemistry and Mineralogy of Bituminous Rocks in Israel. Unpublished Ph.D.. The Hebrew University of Jerusalem., Israel.

Talesnick, M., Hatzor, Y., Tsesarsky, M., 2001. The elastic deformability and strength of a high porosity, anisotropic chalk. Int. J. Rock Mech. Min. Sci. 38 (4), 543–555.

Vernik, L., Landis, C., 1996. Elastic anisotropy of source rocks: implications for hydrocarbon generation and primary migration. AAPG Bull. 80 (4), 531–544.

Vernik, L., Milovac, J., 2011. Rock physics of organic shales. Lead. Edge 30 (3), 318–323.

Vernik, L., Nur, A., 1992. Ultrasonic velocity and anisotropy of hydrocarbon source rocks. Geophysics 57 (5), 727–735.

Wang, Z., Wang, H., Cates, M.E., 1998. Elastic properties of solid clays. In: Paper Presented at the SEG Annual Meeting, New Orleans, pp. 13–18.

Yan, F., Han, D., 2011. Theoretical Validation of Fluid Substitution by Hashin-shtrikman Bounds. San Antonio, pp. 2251–2255.

Yan, F., Han, D., 2013. Measurement of elastic properties of kerogen. In: Paper Presented at the 2013 SEG Annual Meeting. Texas, Houston. http://dx.doi.org/10.1190/segam2013-1319.1.

Zoback, M.D., 2010. Reservoir Geomechanics. Cambridge University Press.